Magnetic resonance imaging techniques for risk stratification in cardiovascular disease

Roes, S.D.

Chapter 3

Correction for heart rate variability during 3D whole heart magnetic resonance coronary angiography

S.D. Roes
G. Korosoglou
M. Schär
J.J.M. Westenberg
M.J.P. van Osch
A. de Roos
M. Stuber

J Magn Reson Imaging 2008;27:1046-1053

Abstract

Purpose

To evaluate the effect of a real-time adaptive trigger delay on image quality to correct for heart rate variability in 3D whole-heart coronary magnetic resonance angiography (MRA).

Materials and methods

Twelve healthy adults underwent 3D whole-heart coronary MRA with and without the use of an adaptive trigger delay. The moment of minimal coronary artery motion was visually determined on a high temporal resolution MRI. Throughout the scan performed without adaptive trigger delay, trigger delay was kept constant, whereas during the scan performed with adaptive trigger delay, trigger delay was continuously updated after each RR-interval using physiological modeling. Signal-to-noise, contrast-to-noise, vessel length, vessel sharpness, and subjective image quality were compared in a blinded manner.

Results

Vessel sharpness improved significantly for the middle segment of the right coronary artery (RCA) with the use of the adaptive trigger delay (52.3 ± 7.1% vs. 48.9 ± 7.9%, $p = 0.026$). Subjective image quality was significantly better in the middle segments of RCA and left anterior descending artery (LAD) when the scan was performed with adaptive trigger delay compared to constant trigger delay.

Conclusion

Our results demonstrate that the use of an adaptive trigger delay to correct for heart rate variability improves image quality mainly in the middle segments of RCA and LAD.

Introduction

Coronary artery disease (CAD) is the leading cause of morbidity and mortality in the Western world, accounting for more than 650 000 deaths each year in the United States (1). Currently, conventional x-ray coronary angiography is the gold standard for detection of coronary artery stenoses and allows for direct visualisation of the coronary artery lumen with high spatial resolution. However, this is an invasive technique accompanied with a small risk of serious complications (2). Furthermore, in a substantial part of the patients referred for coronary angiography, no evidence of clinically important CAD is observed (3). Therefore, a noninvasive test for evaluation of the coronary arteries is warranted. Kim et al. (4) demonstrated that 3-dimensional (3D) coronary magnetic resonance angiography (MRA) enables accurate detection of significant CAD of the proximal and middle segments of the coronary arterial system. However, results from several studies showed that fewer middle coronary segments compared to proximal segments were available for analysis due to inferior image quality, attributable to coronary motion (5,6). Therefore, further improvement of image quality is important and may be achieved by further improvement in coronary motion suppression. Motion of the coronary arteries is caused by respiration as well as by intrinsic myocardial motion. Artifacts caused by respiratory motion can be minimized by the use of navigator-gated techniques (7-11). To account for intrinsic cardiac motion, data acquisition is generally limited to mid-diastole, the most quiescent period in the cardiac cycle (12,13). However, this temporal position (trigger delay) of the cardiac rest period is relative to the R-wave of the electrocardiogram (ECG). The trigger delay is dependent on heart rate and is subject to change in the presence of heart rate variability, which can be observed in most individuals (14). Thus, a heart rate-dependent adjustment of the trigger delay during the scan may further improve motion suppression. The purpose of the present study was the implementation and evaluation of a real-time adaptive trigger delay to correct for heart rate variability in 3D whole-heart in vivo coronary MRA.

Materials and methods

Background

Physiology of the cardiac rest period

The duration of systole and diastole is reduced with increasing heart rates. However, the duration of systole shortens much less than that of diastole (15,16). The most quiescent period of the cardiac cycle is typically found in mid-diastole. Its duration has an inverse relationship with the heart rate: it shortens when the heart rate increases (17). Therefore, the position (and duration) of the cardiac rest period within the cardiac cycle is affected by heart rate variability.

For cardiovascular magnetic resonance imaging (MRI), data acquisition is often synchronized with the cardiac cycle. The synchronization is accomplished by means of triggering the MRI data acquisition to the R-wave of the ECG (18). While information collected from the ECG during triggered cardiac MRI can be used to determine the cardiac rest period, this is not commonly done at the present time. On the ECG, the QT-interval represents the total ventricular systole and is measured from the beginning of the QRS-complex to the end of the T-wave (19). Consequently, the RR-interval minus the QT-interval represents the diastolic portion of the cardiac cycle (Figure 1).

Figure 1.

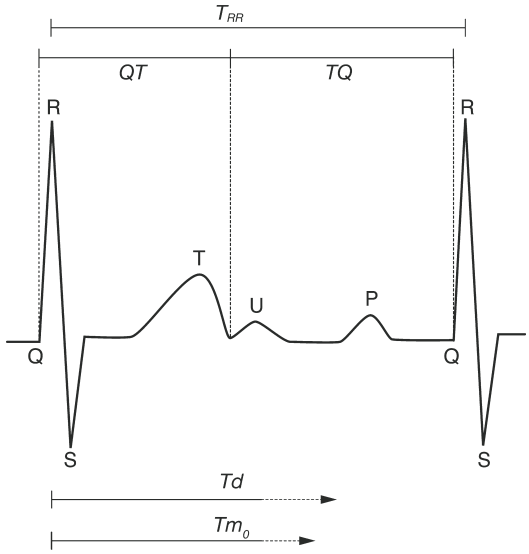

Schematic view of the electrocardiogram and its relation with trigger delay and moment of minimal coronary motion.
Td: trigger delay, Tm_0: moment of minimal coronary motion. T_{RR}: Duration of RR-interval, *TQ*: diastole, *QT*: systole

The nonlinear inverse relationship between QT-interval (systole) and increasing heart rate can be described with the following equation (20):

$$QT = k_1 \cdot \log(10 \cdot (T_{RR} + k_2)) \quad \textbf{(1)}$$

In this equation, k_1 is 0.375 for young men and children, 0.385 for women aged 15-32 years, 0.380 for men aged > 45 years and 0.390 for women aged > 45 years and k_2 is 0.07 (20). Additional analyses by Ashman (21) revealed that in a population with heart disease, a k-value of 0.410 or 0.405 should be used in female and male patients, respectively. T_{RR} represents the time between subsequent R-waves of the ECG. Therefore, the duration of diastole (*TQ*) can be defined as: $T_{RR} - QT$.

The aim of this work was to study the influence of an RR duration dependent real-time adaptive trigger delay on image quality for 3D whole-heart coronary MRA. We hypothesized that the use of continuously adapted trigger delay leads to an improved image quality.

Real-time adaptive trigger delay

Since coronary MRA data collection is performed using segmented k-space approaches, data acquired during *n* RR-intervals with individual durations $T_{RR}(i)$ ($i = 1..n$) contribute to the final image. To account for variability in the RR duration (T_{RR}) during the scan, the average of the 5 latest T_{RR} values was continuously computed and is denoted as $T_{RR,Avg}(i)$.

$$T_{RR,Avg}(i) = \tfrac{1}{i} \sum_{m=1}^{i} T_{RR_m}; \quad for \quad 1 \le i < 5 \quad \textbf{(2)}$$

$$T_{RR,Avg}(i) = \tfrac{1}{5} \sum_{m=i-4}^{i} T_{RR_m}; \quad for \quad 5 \le i \le n \quad \textbf{(3)}$$

With the heart rate-dependent duration of the QT-interval:

$$QT(i) = k_1 \cdot \log(10 \cdot (T_{RR,Avg}(i) + k_2)) \quad \textbf{(4)}$$

The diastolic duration is

$$TQ(i) = T_{RR,Avg}(i) - QT(i) \quad \textbf{(5)}$$

The trigger delay *Td(i)* can be computed in run-time on the scanner as

$$Td(i) = \left\{ \frac{(Tm_0 - QT_0)}{TQ_0} \cdot TQ(i) \right\} + QT(i) \quad \textbf{(6)}$$

In Equation 6, the constant Tm_0 refers to the time delay between the R-wave of the ECG and the onset of the diastolic period of minimal coronary motion of the RCA as was visually determined on high temporal resolution cine images in a horizontal long-axis view that precede 3D whole-heart coronary MRA. Although the three major coronary arteries each have different motion patterns and only partly overlapping rest periods, the middle segment of the right coronary artery (RCA) was analyzed, since in previous studies, the most significant coronary artery displacement was observed in this coronary segment, and this segment also appeared to have the shortest period of minimal motion (17). Importantly, this time-period overlaps with the moment of minimal motion of the proximal, middle and distal segments of all three major coronary arteries (17). Therefore, we hypothesized that by identifying Tm_0 of the RCA at a mid-ventricular level, an adequate timepoint for minimizing coronary motion in general was utilized. Using the average RR duration of this cine scan, the constants QT_0 and TQ_0 (in Equation 6) are computed using the Equations 4 and 5. In run-time and during coronary MRA, *Td(i)* is continuously updated after each RR-interval by using Equations 2 - 6 (Figure 2).

Figure 2.

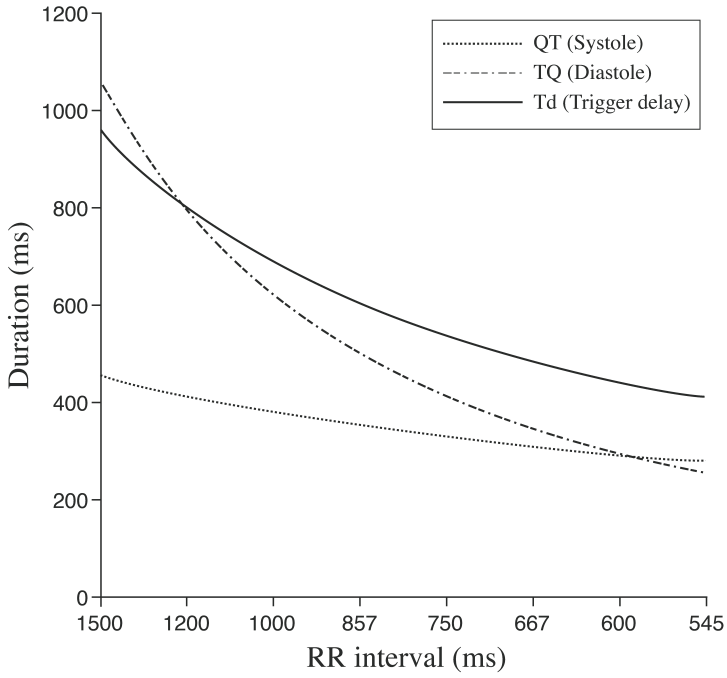

Predicted duration of systole, diastole, and trigger delay as a function of the RR-interval. Predicted duration of systole calculated following Equation 4. The RR-interval duration minus systole (*QT*) represents diastole (*TQ*). For this example, the moment of least coronary motion (*Tm*) was set to 650 ms with k_1 = 0.380 and k_2 = 0.07 (20). Trigger delay (*Td*) is defined by Equation 6.

Study population

Twelve healthy adult subjects (4 males and 8 females, mean age 23.3 ± 4.1 years) without a prior history of cardiac disease were enrolled in the study. For studying this group, we utilized a k_1 value of 0.380. Informed consent was obtained in each subject and the protocol was approved by the hospital's medical ethics committee.

MRI Protocol

MRI studies were performed on a clinical 1.5T Gyroscan ACS-NT MRI scanner (Philips Medical Systems, Best, The Netherlands) equipped with Power Track 6000 gradients. The study subjects were positioned in supine position and data were acquired using vector ECG gating (18). A diagram illustrating the MRI protocol is shown in Figure 3.

Figure 3.

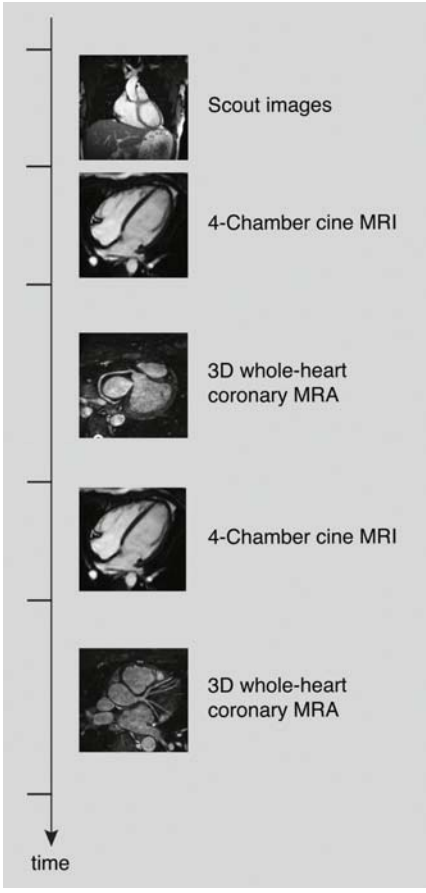

Diagram illustrating the MRI examination.
The 3D whole-heart coronary MRA was performed with and without real-time adaptive trigger delay in random order to avoid bias due to fatigue.

To determine the onset of the period of minimal coronary motion (Tm_0), a free breathing, retrospectively ECG-gated, 2D cine balanced turbo field echo (bTFE) scan in horizontal long-axis view (4-chamber) was performed preceding each 3D whole-heart coronary MRA. Parameters for the cine scan were a field of view of 320 × 320 mm², acquisition matrix of 160 × 160 pixels, slice thickness of 8 mm, flip angle of 60°, echo time of 1.4 ms, and repetition time of 2.9 ms. Temporal resolution was 20 to 30 ms dependent on individual heart rate.

For imaging of the coronary arteries the whole heart was imaged from apex to base with a free-breathing, navigator gated and corrected (gating window of 7 mm), cardiac-triggered, 3D bTFE sequence using one stack with approximately 55 slices, without arrhythmia rejection. A T2 preparation pulse (22) (echo time 50 ms) and fat suppression for contrast generation preceded the imaging part of the sequence. Parameters were a field of view of 270 × 270 mm², acquisition matrix of 272 × 272 pixels, slice thickness of 2 mm, flip angle of 110°, echo time of 2.6 ms, repetition time of 5.2 ms, 23 radiofrequency (RF) excitations per RR-interval and 4 dummy RF pulses were applied to obtain steady-state conditions. The acquisition window was 120 ms. The acquisition duration of the 3D whole-heart coronary MRA was registered. Furthermore, heart frequency was monitored during the 3D whole-heart coronary MRA and RR variability was used as a measure of heart rate variability and was computed as the standard deviation of the RR-interval.

Heart rate variability correction

Before each 3D whole-heart coronary MRA, the above-described cine scans were acquired to visually identify the onset of the mid-diastolic rest period (= Tm_0). Thereby, the timepoint of minimal RCA displacement was determined.

In each volunteer, the 3D whole-heart coronary MRA was performed twice with two different techniques in random order to avoid bias due to fatigue effects. These techniques included:

1) **Non-adaptive trigger delay**: On the cine images, Tm_0 was identified as described above. This time point was used as *Td* and was kept constant throughout the entire 3D whole-heart coronary MRA data acquisition.
2) **Adaptive trigger delay**: On the cine images, the *Td* was determined as for the whole-heart scan without adaptive trigger delay. However, during the 3D whole-heart coronary MRA, *Td* was continuously adjusted (nonlinearly) for heart rate variability as described above.

Data analysis

Quantitative data

The "SoapBubble" tool was used to quantify signal-to-noise ratio (SNR) for blood and muscle, contrast-to-noise ratio (CNR), vessel length, and vessel sharpness (23).

SNR for the blood signal was calculated by measuring the signal intensity in a manually defined region of interest (ROI) in the blood pool of the root of the aorta near the offspring of the corresponding coronary artery and dividing this value by the standard deviation (SD) of the signal from an ROI anterior to the chest wall. For the calculation of SNR in the myocardium, signal intensity was measured in an ROI in the myocardium at the level of the proximal corresponding artery and divided by the SD of the signal in the ROI anterior to the chest wall. CNR was defined as the difference of the mean signal intensities in the ROIs in the blood pool and in myocardium divided by the SD found in the ROI anterior to the chest wall. SNR and CNR were computed for the left and right coronary system separately and the overall SNR and CNR of the scan were calculated (average values of left and right coronary system together). Vessel length was measured on 2D multiplanar reformats (MPR) of the 3D datasets. Length measurements were performed for both the left anterior descending coronary artery (LAD) and the RCA. Vessel sharpness was calculated using a Deriche filter (24) in the proximal and middle coronary segments as previously described (4): the left main coronary artery (LM) and the proximal and middle segments of the LAD (0 to 2 cm and 2 to 4 cm), the left circumflex coronary artery (LCX) (0 to 1.5 cm and 1.5 to 3 cm), and the RCA (0 to 2 cm and 2 to 5 cm). The LM and the proximal LAD were combined (total length of 4 cm) because of the high variability of length, shape and spatial orientation of the LM.

Subjective image quality

Three-dimensional whole-heart coronary MRA data were visually analysed on an Easy Vision 4 workstation (Philips Medical Systems, Best, The Netherlands) in random order by two independent observers who were blinded to the trigger delay technique used. Image quality of the three main coronary arteries was evaluated separately for each coronary artery and for different anatomical levels (proximal, middle and distal segments). The coronary segments were scored using a 5-point scale as previously described (8): 0: coronary artery not visible, 1: coronary artery visible with markedly blurred borders or edges, 2: coronary artery visible with moderately blurred borders or edges, 3: coronary artery visible with mildly blurred borders or edges, 4: coronary artery visible with sharply defined borders or edges.

Statistical Analysis

Continuous data are expressed as mean ± SD. Differences in quantitative and qualitative data between the two scan methods were analyzed using the Wilcoxon signed ranks test. A p-value of < 0.05 was considered statistically significant.

Results

The MRI protocol was successfully completed in all 12 examined subjects. However, one volunteer was excluded from the data analysis because of overall poor image quality caused by ECG-triggering problems.

The mean duration of the 3D whole-heart coronary MRA was 17.6 ± 4.6 minutes dependent on individual heart rate and navigator efficiency. No significant difference in acquisition duration was observed between scans performed with constant trigger delay and adaptive trigger delay (17.4 ± 4.9 and 17.8 ± 4.5 minutes, respectively, $p = 0.7$). The mean heart rate of the volunteers during acquisition of the 3D whole-heart coronary MRA was 64 ± 9 bpm with a mean RR variability of 61 ± 22 ms. No significant differences in heart frequency and RR variability were observed during scans performed with constant and adaptive trigger delay (Table 1).

Table 1. Scanning duration of 3D whole-heart coronary MRA, heart rate and RR variability (SD of RR-interval) in scans performed with constant trigger delay and real-time adaptive trigger delay.

	Constant trigger delay	Real-time adaptive trigger delay	P-value
Scan duration (min)	17.4 ± 4.9	17.8 ± 4.5	0.7
Heart rate (bpm)	64 ± 10	64 ± 9	0.7
RR variability (ms)	62 ± 21	59 ± 23	0.3

Data are expressed as mean ± SD.

Quantitative data

Results from quantitative data analysis are shown in Tables 2 and 3. Vessel sharpness was significantly higher (improved) in the middle segment of the RCA when the adaptive trigger delay was used (52.3 ± 7.1 vs. 48.9 ± 7.9, $p = 0.026$).

A trend towards higher muscle signal (13.1 ± 3.6 vs. 11.0 ± 4.2, $p = 0.08$) and longer visualized vessel length of the LAD (112.1 ± 28.8 vs. 108.1 ± 32.6, $p = 0.07$) was observed in scans performed with adaptive trigger delay as compared with those obtained with constant trigger delay. Furthermore, overall muscle signal was significantly higher when scans were performed with adaptive trigger delay (12.9 ± 3.3 vs. 11.0 ± 3.1, $p = 0.041$).

Table 2. Vessel sharpness for 3D whole-heart coronary MRA performed with constant trigger delay and real-time adaptive trigger delay.

	Constant trigger delay	Real-time adaptive trigger delay	P-value
Vessel sharpness (%)			
LM + proximal segment LAD	41.8 ± 8.6	43.0 ± 6.8	0.8
Proximal segment LCX	49.4 ± 9.4	44.8 ± 6.5	0.09
Proximal segment RCA	54.4 ± 9.5	56.6 ± 8.7	0.4
Middle segment LAD	42.7 ± 10.7	43.2 ± 12.0	0.7
Middle segment LCX	44.4 ± 7.5	44.0 ± 6.6	0.7
Middle segment RCA	48.9 ± 7.9	52.3 ± 7.1	0.026

Data are expressed as mean ± SD.
LM: left main coronary artery, LAD: left anterior descending coronary artery, LCX: left circumflex coronary artery, RCA: right coronary artery.

Table 3. Results from quantitative data analysis of the 3D whole-heart coronary MRA performed with constant trigger delay and real-time adaptive trigger delay.

	Constant trigger delay	Real-time adaptive trigger delay	P-value
Left coronary system			
SNR (muscle)	11.0 ± 4.2	13.1 ± 3.6	0.08
SNR (blood)	20.2 ± 6.2	22.7 ± 5.3	0.5
CNR	9.1 ± 4.6	9.5 ± 3.6	0.8
Length (mm)	108.1 ± 32.6	112.1 ± 28.8	0.07
Right coronary system			
SNR (muscle)	11.1 ± 3.2	12.7 ± 3.9	0.1
SNR (blood)	27.2 ± 7.5	28.8 ± 6.7	0.5
CNR	16.0 ± 5.5	16.1 ± 3.4	1.0
Length (mm)	136.1 ± 55.2	134.7 ± 46.8	1.0
Left and right coronary system combined			
SNR (muscle)	11.0 ± 3.1	12.9 ± 3.3	0.041
SNR (blood)	23.7 ± 6.2	25.7 ± 4.7	0.3
CNR	12.6 ± 4.7	12.8 ± 2.6	0.8

Data are expressed as mean ± SD. CNR: contrast-to-noise ratio, SNR: signal-to-noise ratio.

Subjective image quality

Results from subjective image quality scoring are presented in Table 4. Image quality was significantly better in the middle segments of the LAD and RCA when the adaptive trigger delay was used. Simultaneously, a trend towards better image quality using the

adaptive trigger delay was found for the proximal segments of all main coronary arteries and the distal part of the LAD. Furthermore, the overall image quality per anatomical level (proximal, middle and distal) was significantly better when scans were performed using the adaptive trigger delay. Figure 4 shows multiplanar reformatted images of the RCA acquired with and without the adaptive trigger delay of a volunteer with high RR variability and a volunteer with low RR variability. More significant improvement of image quality is observed in the volunteer with high RR variability.

Discussion

In the present work, we developed, implemented and tested the utility of a real-time adaptive trigger delay for improved 3D whole-heart coronary MRA. Our results suggest that the use of an adaptive trigger delay results in a significantly improved quantitative and qualitative image quality mainly in the middle segments of both the RCA and LAD.

Table 4. Results from consensus image quality scoring of the 3D whole-heart coronary MRA obtained constant trigger delay and real-time adaptive trigger delay.

	Constant trigger delay	Real-time adaptive trigger delay	P-value
Proximal segments			
LM	2.5 ± 0.9	2.9 ± 0.7	0.10
LAD	2.6 ± 1.2	3.1 ± 0.8	0.06
LCX	2.6 ± 1.1	2.9 ± 0.9	0.08
RCA	3.0 ± 0.8	3.6 ± 0.9	0.06
Overall proximal segments	2.7 ± 1.0	3.1 ± 0.9	< 0.001
Middle segments			
LAD	2.5 ± 1.2	3.0 ± 0.8	0.034
LCX	1.9 ± 0.8	2.3 ± 0.8	0.10
RCA	2.7 ± 1.0	3.4 ± 0.9	0.038
Overall middle segments	2.4 ± 1.1	2.9 ± 0.9	< 0.001
Distal segments			
LAD	1.3 ± 1.3	1.7 ± 1.2	0.06
LCX	1.0 ± 1.3	1.1 ± 1.3	0.3
RCA	2.2 ± 1.3	2.5 ± 1.4	0.3
Overall distal segments	1.5 ± 1.3	1.8 ± 1.4	0.021

Data are expressed as mean ± SD.
LM: left main coronary artery, LAD: left anterior descending coronary artery, LCX: left circumflex coronary artery, RCA: right coronary artery.

Figure 4.

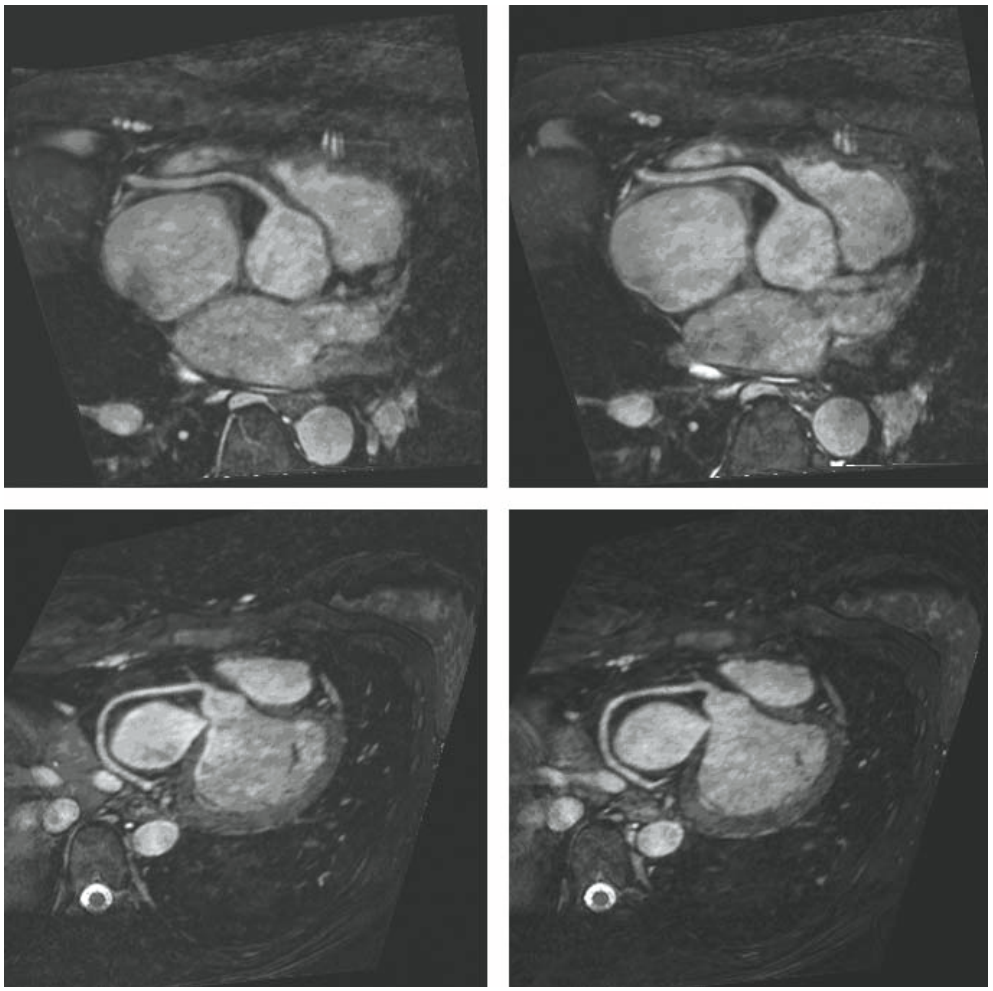

Multiplanar reformatted MR images of the RCA from a volunteer with high heart rate variability (SD of RR-interval was 103 ms). The 3D whole heart coronary MRA was performed with constant trigger delay (upper left) and real-time adaptive trigger delay (upper right). Note the improved image quality mainly in the middle segment of the RCA.
Multiplanar reformatted MR images of the RCA of a volunteer with low heart rate variability (standard deviation of RR-interval was 45 ms) acquired using constant trigger delay (lower left) and real-time adaptive trigger delay (lower right). Note that there is a slight improvement in image quality.

Since contemporary coronary MRA techniques do not permit 3D real-time data collection with sufficient temporal and spatial resolution, k-space segmentation is mandatory. However, k-space segmentation critically depends upon the quality and reproducibility of the spatial registration between the imaged volume and the coronary arteries. To ensure the reproducibility of this geometric condition over many heartbeats

and respiratory cycles, motion suppression techniques such as breath-holding, respiratory navigators and ECG triggering have been used. Simultaneously, it has been increasingly recognized that adverse effects of cardiac motion during the data collection period (= acquisition interval) can be minimized by imaging during the most quiescent period in the cardiac cycle (25-28). While this quiescent period can be identified on cine scans using visual or automated approaches (29,30), the temporal position of this 'window of opportunity' relative to the R-wave of the ECG is still subject to change as a function of the RR duration. And since changes in the duration of the RR-interval occur in most subjects (14), the goal of this work was the implementation of a real-time adaptive shift of the position of the data collection period within the RR-interval for improved whole-heart coronary MRA. Since earlier ECG studies revealed that the relative duration of both systole and diastole does not scale linearly with the RR duration (20, 31-33) a simple linear shift of the position of the acquisition window as a function of the RR duration did not seem adequate. Therefore, we implemented a non-linear adaptive trigger delay for RR duration dependent positioning of the acquisition interval relative to the R-wave of the ECG. Using this implementation, the hypothesis was tested whether real-time adaptation of the temporal position of the acquisition interval leads to improved image quality in 3D whole-heart coronary MRA.

Consensus reading by two blinded and experienced observers showed a significant improvement in image quality mainly for the middle segments of the RCA and LAD. This improved image quality was confirmed by objective quantitative data analysis: overall vessel sharpness was significantly better in the middle segment of the RCA when using the adaptive trigger delay. The beneficial effect of the adaptive trigger delay in these coronary segments might be related to the movement pattern of the coronary artery tree. Johnson et al. (17) studied the 3D motion of the coronary arteries and found that the largest total coronary displacement of 16.08 mm was observed in the middle segment of the RCA. The maximum displacement of the LAD was also observed in the middle segment. Consequently and consistent with our findings, it is expected that these middle segments profit most from adaptation of the temporal position of the acquisition window.

The fact that middle segments benefit from an adaptive trigger delay may be important since especially proximal CAD could be reliably identified thus far using coronary MRA. Therefore, trigger delay adaptation may support the identification of significant CAD in middle segments of the coronary arteries as well.

Since the 3D whole-heart scans with and without the adaptive trigger delay were acquired with the same imaging parameters, no major improvement in SNR and CNR was expected. However, a trend towards higher muscle signal for the left and right coronary system separately and a significant improvement of overall muscle signal was observed for scans acquired with adaptive trigger delay. This may be attributed to reduced myocardial motion.

In accordance to most previous studies, data were acquired in diastole, typically the most quiescent period in the cardiac cycle (4, 17, 25). However, a more recent study suggests that imaging at end-systole does not affect image quality if the acquisition window is SENSE abbreviated (34). Especially in tachycardic patients, imaging at end-systole (using equation 1) may be valuable but remains to be investigated.

In the current study, the scanning time for free-breathing 3D whole-heart coronary MRA was relatively long in comparison to other, more recent studies using similar methodology (35). This prolonged scanning time is attributable to the fact that no parallel imaging was used in our study. While SENSE acceleration could have been used, SNR and CNR computations would not have been adequate. Therefore, no SENSE was applied in the current study, but it is expected that accelerated scans will equally benefit for real-time adapted trigger delay.

Plein et al. (28) evaluated a subject-specific acquisition window, in combination with motion-adapted respiratory gating and observed shorter scanning times while maintaining image quality. Implementing a real-time adaptive acquisition window in combination with a real-time adaptive trigger delay seems a logical next step that involves a challenging engineering task, but this was beyond the scope of our current study.

Limitations of the present study include the relatively small number of subjects that were studied and the fact that the real-time adaptation of the trigger delay always utilized the duration of the 5 preceding RR-intervals for adaptation. While this approach accounts for relatively slow changes in the RR duration, the optimal number of RR intervals that are needed for adaptation remains to be identified. Simultaneously, sudden changes in heart rate induced by ectopic beats, swallowing (36) or arrhythmia, constitute additional sources of RR variability and image artefacts, which cannot be easily accounted for by the current algorithm. However, by using arrhythmia rejection algorithms (37), some of these adverse effects on image quality can be minimized, albeit at the cost of prolonged scanning time. Furthermore, while the 3D whole-heart acquisitions support the visualisation of prolonged coronary segments when compared to earlier volume targeted approaches, the analysis tools that are currently available remain to be adapted for adequate quantitative analysis of the entire vessel length. In addition, the adult subjects that were studied are relatively young and age progression has shown to be related to decreased heart rate variability (14). However, regardless of age, a slow drift in heart rate is commonly observed in both patients and healthy adult subjects during the scans, and our algorithm is capable of compensating for this.

In conclusion, the use of a real-time adaptive positioning of the data collection period within the RR-interval results in improved image quality for contemporary 3D whole-heart coronary MRA approaches in a cohort of healthy adult subjects. The main improvement in image quality was observed for the middle segments of both RCA and LAD.

References

1. Thom T, Haase N, Rosamond W, et al. Heart Disease and Stroke Statistics-2006 Update: A Report From the American Heart Association Statistics Committee and Stroke Statistics Subcommittee. Circulation 2006;113:85-151.
2. Scanlon PJ, Faxon DP, Audet AM, et al. ACC/AHA Guidelines for Coronary Angiography. A Report of the American College of Cardiology/American Heart Association Task Force on Practice Guidelines (Committee on Coronary Angiography). Developed in Collaboration With the Society for Cardiac Angiography and Interventions. J Am Coll Cardiol 1999;33:1756-1824.
3. Budoff MJ, Georgiou D, Brody A, et al. Ultrafast Computed Tomography As a Diagnostic Modality in the Detection of Coronary Artery Disease: a Multicenter Study. Circulation 1996;93:898-904.
4. Kim WY, Danias PG, Stuber M, et al. Coronary Magnetic Resonance Angiography for the Detection of Coronary Stenoses. N Engl J Med 2001;345:1863-1869.
5. Kim RJ, Wu E, Rafael A, et al. The Use of Contrast-Enhanced Magnetic Resonance Imaging to Identify Reversible Myocardial Dysfunction. N Engl J Med 2000;343:1445-1453.
6. van Geuns RJ, Wielopolski PA, de Bruin HG, et al. MR Coronary Angiography With Breath-Hold Targeted Volumes: Preliminary Clinical Results. Radiology 2000;217:270-277.
7. Jahnke C, Paetsch I, Schnackenburg B, et al. Coronary MR Angiography With Steady-State Free Precession: Individually Adapted Breath-Hold Technique Versus Free-Breathing Technique. Radiology 2004;232:669-676.
8. McConnell MV, Khasgiwala VC, Savord BJ, et al. Comparison of Respiratory Suppression Methods and Navigator Locations for MR Coronary Angiography. AJR Am J Roentgenol 1997;168:1369-1375.
9. Oshinski JN, Hofland L, Mukundan S Jr, et al. Two-Dimensional Coronary MR Angiography Without Breath Holding. Radiology 1996;201:737-743.
10. van Geuns RJ, de Bruin HG, Rensing BJ, et al. Magnetic Resonance Imaging of the Coronary Arteries: Clinical Results From Three Dimensional Evaluation of a Respiratory Gated Technique. Heart 1999;82:515-519.
11. Fischer RW, Botnar RM, Nehrke K, et al. Analysis of Residual Coronary Artery Motion for Breath Hold and Navigator Approaches Using Real-Time Coronary MRI. Magn Reson Med 2006;55:612-618.
12. Hofman MB, Wickline SA, Lorenz CH. Quantification of in-Plane Motion of the Coronary Arteries During the Cardiac Cycle: Implications for Acquisition Window Duration for MR Flow Quantification. J Magn Reson Imaging 1998;8:568-576.
13. Wang Y, Vidan E, Bergman GW. Cardiac Motion of Coronary Arteries: Variability in the Rest Period and Implications for Coronary MR Angiography. Radiology 1999;213:751-758.
14. Ravenswaaij-Arts CM, Kollee LA, Hopman JC, et al. Heart rate variability. Ann Intern Med 1993;118:436-47.
15. Katz AM. The working heart. Physiology of the heart. New York: Raven Press; 1977. p 209-227.
16. Sherwood L. Cardiac physiology. Lewis, P. Human physiology: from cells to systems. 3 ed. Belmont: Wadsworth Publishing Company; 1997. p 265-304.

17. Johnson KR, Patel SJ, Whigham A, et al. Three-Dimensional, Time-Resolved Motion of the Coronary Arteries. J Cardiovasc Magn Reson 2004;6:663-673.
18. Fischer SE, Wickline SA, Lorenz CH. Novel Real-Time R-Wave Detection Algorithm Based on the Vectorcardiogram for Accurate Gated Magnetic Resonance Acquisitions. Magn Reson Med 1999;42:361-370.
19. Electrical activity of the heart- Recordings from the body surface. In: Lentner C, editor. Geigy Scientific Tables, volume 5, Heart and Circulation. 8th edition. West Caldwell, NJ: Ciby-Geigy corporation; 1990. p 143.
20. Ashman R, Hull E. The normal human electrocardiogram and changes produced by disease. The T wave, the Q-T interval, and the U wave. In: Essentials of electrocardiography for the student and practitioner of medicine. 2nd edition. New York: The Macmillan Company; 1945. p 162-163.
21. Ashman R. The normal duration of the Q-T interval. Am Heart J 1942:23:522-534.
22. Brittain JH, Hu BS, Wright G A, et al. Coronary Angiography With Magnetization-Prepared T2 Contrast. Magn Reson Med 1995;33:689-696.
23. Etienne A, Botnar RM, Van Muiswinkel AM, et al. "Soap-Bubble" Visualization and Quantitative Analysis of 3D Coronary Magnetic Resonance Angiograms. Magn Reson Med 2002;48:658-666.
24. Botnar RM, Stuber M, Danias PG, et al. Improved Coronary Artery Definition With T2-Weighted, Free-Breathing, Three-Dimensional Coronary MRA. Circulation 1999;99:3139-3148.
25. Kim WY, Stuber M, Kissinger KV, et al. Impact of Bulk Cardiac Motion on Right Coronary MR Angiography and Vessel Wall Imaging. J Magn Reson Imaging 2001;14:383-390.
26. Wang Y, Watts R, Mitchell I, et al. Coronary MR Angiography: Selection of Acquisition Window of Minimal Cardiac Motion With Electrocardiography-Triggered Navigator Cardiac Motion Prescanning--Initial Results. Radiology 2001;218:580-585.
27. Jahnke C, Paetsch I, Achenbach S, et al. Coronary MR Imaging: Breath-Hold Capability and Patterns, Coronary Artery Rest Periods, and Beta-Blocker Use. Radiology 2006;239:71-78.
28. Plein S, Jones TR, Ridgway JP, et al. Three-Dimensional Coronary MR Angiography Performed With Subject-Specific Cardiac Acquisition Windows and Motion-Adapted Respiratory Gating. AJR Am J Roentgenol 2003;180:505-512.
29. Jahnke C, Paetsch I, Nehrke K, et al. A New Approach for Rapid Assessment of the Cardiac Rest Period for Coronary MRA. J Cardiovasc Magn Reson 2005;7:395-399.
30. Ustun A, Desai M, Abd-Elmoniem KZ, et al. Automated Identification of Minimal Myocardial Motion for Improved Image Quality on MR Angiography at 3 T. AJR Am J Roentgenol 2007;188:W283-W290.
31. Bazett HC. An Analysis of the Time-Relations of Electrocardiograms. Heart 1920;7:353.
32. Hegglin R, Holzmann, M. Die Klinische Bedeutung Der Verlänerten QT-Distanz (Systolendauer) Im Elektrokardiogramm. Ztschr klin Med 1937;132:1.

33. Schlomka G, Raab W. Zur. Bewertung Der Relativen Systolendauer; Über Die Abhängigkeit Der Relativen Systolendauer Des Gesunden Vom Lebensalter. Ztschr Kreislaufforsch 1933;28:673.
34. Gharib AM, Herzka DA, Ustun AO, et al. Coronary MR Angiography at 3T During Diastole and Systole. J Magn Reson Imaging 2007;26:921:926.
35. Sakuma H, Ichikawa Y, Chino S, et al. Detection of Coronary Artery Stenosis With Whole-Heart Coronary Magnetic Resonance Angiography. J Am Coll Cardiol 2006;48:1946-1950.
36. Sherozia OP, Ermishkin VV, Lukoshkova EV. Dynamics of Swallowing-Induced Cardiac Chronotropic Responses in Healthy Subjects. Bull Exp Biol Med 2003;135:322-326.
37. Leiner T, Katsimaglis G, Yeh EN, et al. Correction for Heart Rate Variability Improves Coronary Magnetic Resonance Angiography. J Magn Reson Imaging 2005;22:577-582.